JOURNAL OF MATERIALS SCIENCE 16 (1981) 3183–3193

Annealing behaviour of amorphous $Fe_{80}B_{20}$ on continuous heating

O. T. INAL, C. V. ROBINO, L. KELLER
Department of Metallurgical and Materials Engineering, New Mexico Institute of Mining and Technology, Socorro, New Mexico 87801, USA

F. G. YOST, M. M. KARNOWSKY
Sandia National Laboratories, Albuquerque, New Mexico 87185, USA

Resistance measurements during direct heating of $Fe_{80}B_{20}$ amorphous alloys indicate phase changes occur at 395, 500, 720 and 840° C. Samples heated to these temperatures, and maintained for five minutes in a neutral atmosphere, show that a hardness maximum occurs at the crystallization temperature of 395° C and that annealing at 500° C produces a material with the same hardness. Above 500° C the microhardness is seen to drop below that of the amorphous alloy. Saturation magnetization measurements show a steady increase following each anneal, up to a temperature of 720° C, and the rate of increase is seen to drop in the range of 720 to 840° C. X-ray diffraction studies show that only a small fraction of the matrix is crystallized following the anneal at 395° C and the transformed phases are α-Fe and Fe_3B. Following annealing at 500° C, an increased proportion of α-Fe and Fe_3B are observed with complete crystallinity while samples heat-treated at 720° C are seen to consist of a three-phase mixture of α-Fe, $Fe_{23}B_6$ and Fe_2B. Annealing at 840° C is seen to produce an equilibrium phase mixture of α-Fe and Fe_2B phases. Only in the sample annealed at 395° C is a fraction of the amorphous phase seen to persist, indicating that a 5 min anneal is not sufficient, at this temperature, to induce complete crystallization. These structural features are corroborated by field ion microscope analyses, made at liquid nitrogen temperature in a medium of pure neon, and scanning electron microscopy, and are also consistent with our earlier study involving the isothermal annealing, for various times, of $Fe_{80}B_{20}$ alloy at 780° C.

1. Introduction

Interest in amorphous alloys stems from the unique combination of properties they possess, including high strength [1], superior corrosion resistance and soft magnetic behaviour [2]. However, proper utilization of these properties has to be based on an understanding of the thermal durability of these alloys and the alterations induced in the aforementioned physical properties with such exposure to elevated temperatures as may occur in their intended applications. Our initial study on the isothermal annealing behaviour of $Fe_{80}B_{20}$ alloy at 780° C reveals that [3]:

(a) this heat treatment leads to a three-stage phase transformation with distinct phase mixtures constituting the microstructure;

(b) the equilibrium phase mixture that is finally achieved, following annealing for 2.25 h, consists of the α-Fe(b c c) and Fe_2B(b c t) phases; and

(c) no discernible incubation period is observed in the phase transformations induced at 780° C and even an anneal of duration 1 sec yields a metastable but totally crystalline phase mixture of Fe_3B and α-Fe. Such extensive changes in microstructure, with heat treatment, should lead to considerable changes in the physical properties mentioned earlier. This study, therefore, attempts to delineate alterations introduced in such physical properties

0022–2461/81/113183–11$03.10/0 © *1981 Chapman and Hall Ltd.*

as microhardness and saturation magnetization, and to correlate these changes to microstructural features attained through direct heating of $Fe_{80}B_{20}$ alloy between ambient temperature and 840° C. For this purpose both sheet and wire samples were annealed at temperatures (obtained from a per cent resistance change against temperature curve) where structural changes were observed and analysed through microhardness testing, saturation magnetization measurements, X-ray diffraction pattern analysis and field ion and scanning electron microscopy.

2. Experimental procedure

The annealing temperatures were selected to correspond to microstructural changes observed on the per cent change in resistance against temperature curve, shown in Fig. 1. Point 1 in this curve is the crystallization temperature, 395° C [4], and Points 2 to 4 correspond to possible phase changes occurring at 500° C, 720° C and 840° C, respectively.

Resistance measurements were made using a four-terminal reversing polarity apparatus with a constant current of 0.1 A being passed through the samples. Platinum current and voltage leads were welded at each end of the sample followed by encapsulation in a quartz tube at a pressure of 100 Torr helium. The per cent change in resistance, R, was determined for each point by normalizing to the dimensionless form [5]:

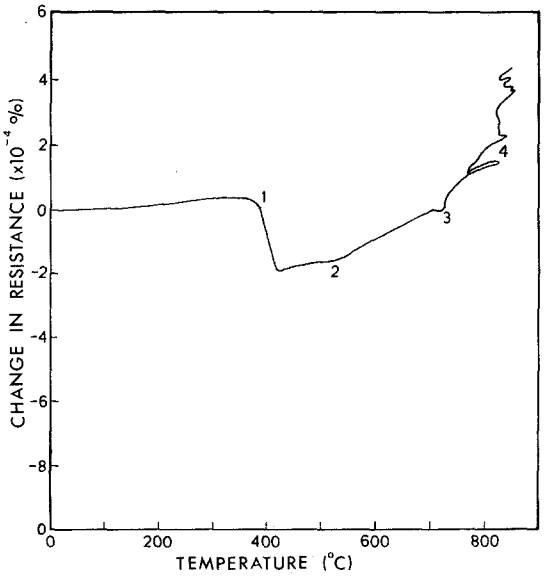

Figure 1 Per cent change in resistance plotted against temperature for $Fe_{80}B_{20}$ metallic glass. The points of inflection used for the various heat treatments in this study are indicated on the curve, Points 1 to 4.

$$\text{Per cent change in } R = \frac{R_i - R_T}{R_0 - R_T} \times 100, \quad (1)$$

where R_i is the instantaneous resistance of any temperature, R_0 is the resistance of the amorphous state and R_T is the resistance at 840° C. Heating was stopped at 840° C since no further points of inflection, indicating a phase change, had been observed above this temperature. Absolute resistivity values were not determined.

Wire samples of diameter 0.075 mm and ribbons of dimensions 25.4 mm x 0.0508 mm were heated in an argon atmosphere, following a purge of 24 h; each sample was held at the chosen experimental temperature for 5 min followed by furnace cooling before evaluation of the structural and physical properties was undertaken.

2.1. Structural analysis

2.1.1. X-ray diffraction

The amorphous and heat-treated wire samples were investigated by the X-ray powder diffraction method using a GE Debye–Scherrer camera with filtered CrKα radiation (at 35 kV and 25 mA). Analyses of the amorphous and heat-treated ribbon samples, on the other hand, were made with the use of the diffractometer technique employing filtered CrKα radiation (at 40 kV and 20 mA) in a Phillips Norelco wide-range diffractometer with a PW 1720 X-ray generator. The data obtained is summarized in Table IA. Table IB lists, for comparison, the results of previous structural studies [3, 6–10] made on the $Fe_{80}B_{20}$ alloy.

2.1.2. Field ion microscopy

The field-emission end forms imaged in this investigation were produced by electro-etching the wire samples in a solution containing 20 vol% HNO_3, 20 vol% HCl and 60 vol% CH_3OH using an alternating current of 1 to 3 V. These samples were imaged at 78 K in a pure neon gas, with continuous titanium gettering, at a background pressure of about 5×10^{-6} Torr. The details of the field ion microscope used in these analyses are given elsewhere [11].

Results of this study are summarized in Table IA and are shown in Figs 2 to 6. Fig. 2 shows the atomic details of a surface in the as-received wire, exhibiting a completely random atomic arrangement of the iron species (since boron atoms do not contribute to the image) [3] with no indication of long-range order, as expected from an amorphous

TABLE IA Structural analysis of $Fe_{80}B_{20}$

Heat treatment (5 min at temperature)	X-ray diffraction pattern result	Unit-cell structure	Field ion microscope observations
Amorphous (as-received)	Amorphous halo		Random atomic distribution, no long-range order
395° C	α-Fe Fe_3B Amorphous	b c c Tetragonal	α-Fe precipitates and Fe_3B in a matrix with a different *BIV*
500° C	α-Fe Fe_3B	b c c Tetragonal	α-Fe precipitates within Fe_3B phase
720° C	α-Fe Fe_2B $Fe_{23}B_6$	b c c Tetragonal f c c	α-Fe in a twin slice with two other phases, one with a higher symmetry
840° C	α-Fe Fe_2B	b c c Tetragonal	Zones of α-Fe and in a matrix of Fe_2B with indications of symmetry

TABLE IB Structural analyses of $Fe_{80}B_{20}$: previous work

Heat treatment	Phase structure observed	Unit-cell structure	Lattice constants (nm)	Reference number
780° C for 1 sec to 15 min	α-Fe Fe_3B	b c c p t	– $a_0 = 0.8623, c_0 = 0.4294$	[3]
780° C for 22.5 min to 1 h	α-Fe Fe_3B Fe_2B	b c c p t b c t	– – –	[3]
780° C for 2.25 h to 8 h	α-Fe Fe_2B	b c c b c t	– –	[3]
300 to 450° C	α-Fe ~ Fe_4B	b c c b c t	– $a = 0.864, c = 0.428$	[6–8]
700 to 800° C	α-Fe Fe_3B	b c c orthorhombic	– $a = 0.543, b = 0.666, c = 0.445$	[6–8]
> 1000° C	α-Fe Fe_2B	b c c –	– –	[6–8]
380° C for 2 h	α-Fe Fe_3B	b c c b c t	– $a = 0.863, c = 0.429$	[9]
300° C for 100 h	α-Fe Fe_3B	b c c b c t	– –	[10]
600° C for 2 h 700° C for 2 h	α-Fe Fe_3B Fe_2B	b c c b c t and orthorhombic	– – –	[10]
900° C for 2 h	α-Fe Fe_2B	– –	– –	[10]

alloy. Fig. 3, on the other hand, shows that an anneal of five minutes at 395° C has produced two precipitate phases, α-Fe and Fe_3B, in a matrix that obviously possesses a different best-image voltage (hence, it is seen as a dark area) consisting possibly of the still amorphous material. Fig. 4 shows the image for the alloy annealed at 500° C and is seen to consist of α-Fe clusters, showing a ring structure and thus higher symmetry of the b c c metal, in a matrix of Fe_3B phase. The structure obtained following heat-treatment at 720° C is shown in Fig. 5. The twin slice, at an angle of approximately 120° to the horizontal, is seen to consist mainly of α-Fe atoms. It is seen to possess more symmetry (in

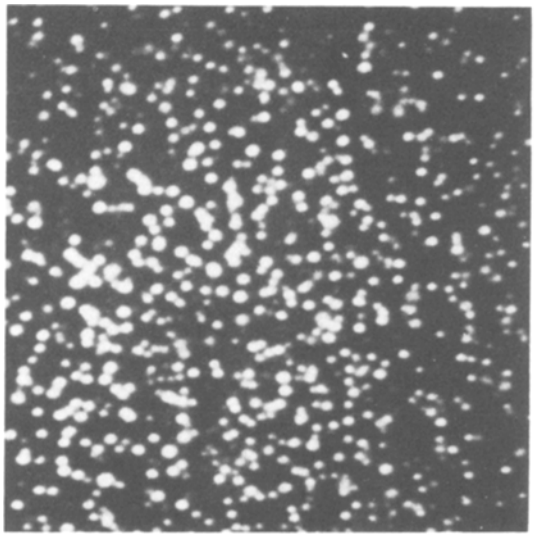

Figure 2 Field ion micrograph of the amorphous (as-received) $Fe_{80}B_{20}$ alloy showing completely random distribution of Fe atoms.

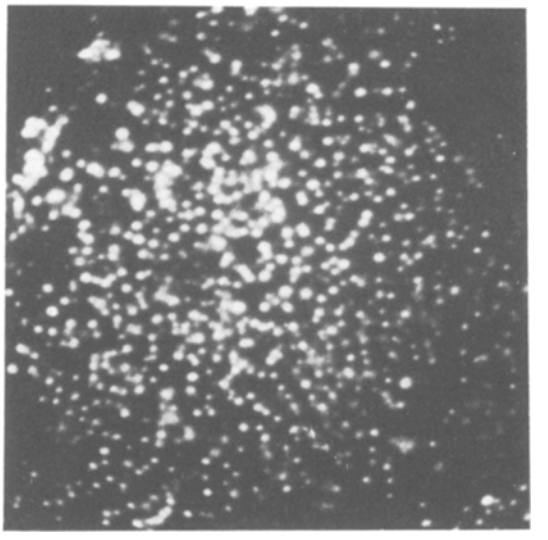

Figure 4 Field ion micrograph of sample annealed for 5 min at 500° C. α-Fe phase clusters (larger spots arranged in the more obvious partial-ring structures) distributed in a matrix of the totally crystallized Fe_3B phase.

the form of partial ring structure) than the phases to either its right or its left. The distinction made here, between Fe_2B and α-Fe, is based on the higher symmetry possessed by α-Fe and is seen in this micrograph in the form of partial ring formation. The micrograph seen in Fig. 6 is that of a sample annealed at 840° C. The bright spots indicating the clustering of α-Fe atoms, at an angle of approximately 45° to the horizontal and running through the micrographs, are seen to separate domains of the Fe_2B phase. The partial ring structure observed in the domains of the Fe_2B phase and the suggestion of higher symmetry in this structure indicate the total disappearance of the Fe_3B phase with this heat treatment of the amorphous wire.

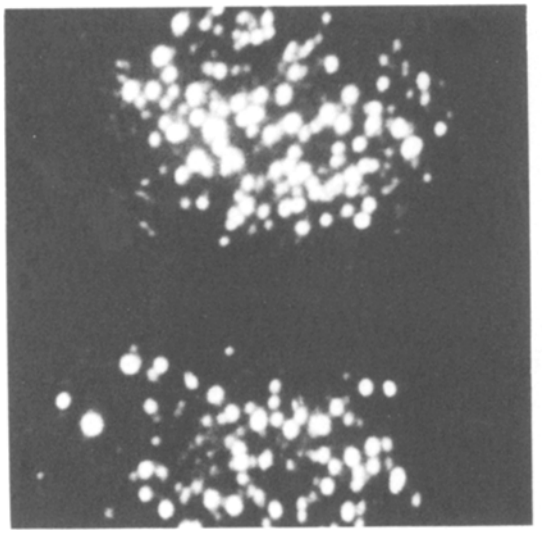

Figure 3 Field ion micrograph of $Fe_{80}B_{20}$ sample following annealing for 5 min at 395° C. α-Fe phase clusters and the Fe_3B phase are shown in a matrix of the uncrystallized matrix with a different best-image voltage (thus seen as the dark zone).

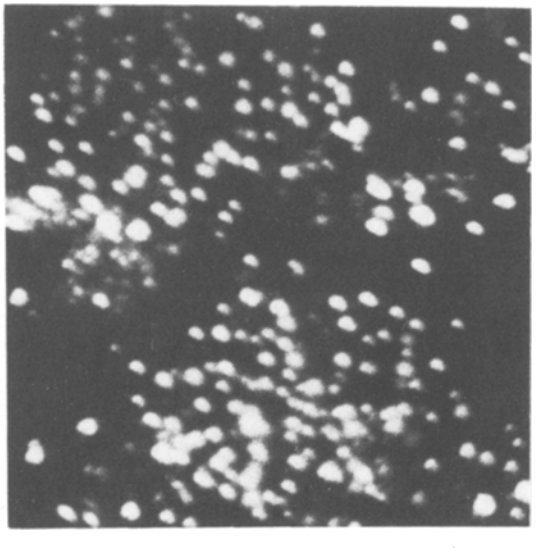

Figure 5 Field ion micrograph of the sample annealed for 5 min at 720° C. A twin slice, at an angle of about 120° to the horizontal, consisting of α-Fe phase atoms, is shown with the phase to the right and to the left exhibiting sparser population of iron atoms and lower symmetry.

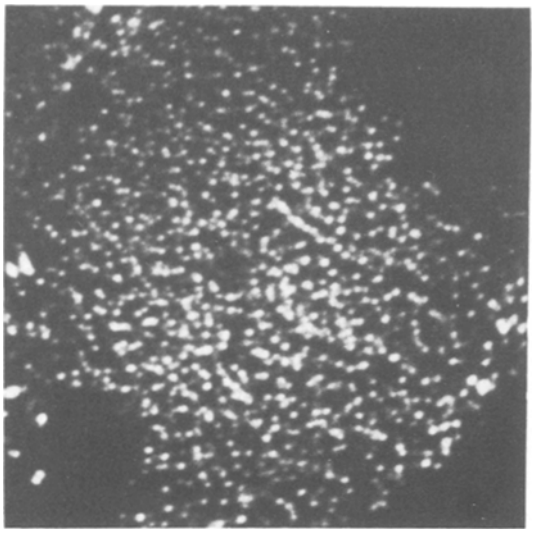

Figure 6 Field ion micrograph of the sample annealed at 840° C for 5 min. Clusters of α-Fe phase atoms are shown separating domains of the Fe_2B phase.

2.1.3. Scanning electron microscopy

Ribbon samples, both before and after annealing treatments, were mounted in a Buehler Epo-Kwick resin (with maximum curing temperature of 80° C) and polished to a finish of 0.06 μm with alumina on a Buehler Rayvel cloth. The polished surfaces were then etched in a solution of 1 vol% HNO_3 in methanol for 10 to 20 sec to delineate the associated structural features. The scanning electron microscope used in this study was a Hitachi–Perkin Elmer, model HHS-2R, instrument operated in the secondary electron emission mode at an accelerating voltage of 25 kV.

Fig. 7a to d shows the microstructure of the heat-treated samples at the lower magnification of the scanning electron microscope for a comparison with the atomistic expose of Figs 2 to 6. Fig. 7a shows the sample annealed to 395° C exhibiting domains of transformed material (Points A and B) in a matrix that is otherwise uniform. A higher magnification was utilized in this micrograph to delineate the difference of colour contrast between the three species present. Fig. 7b shows the microstructure of the sample following anneal to 500° C and although this magnification is not sufficient to delineate the phases present, it can be seen that the surface is quite uniform. Fig. 7c shows the sample surface following heating to 720° C where two product phases (Regions A and B) are seen to be imbedded in the matrix phase. The contrast afforded by the etch used on these surfaces distinguishes the two product phases from the matrix. Finally, Fig. 7d shows the equiaxed grains of the matrix phase to be separated by a transformation product in the sample annealed at 840° C.

2.2. Physical property evaluations

2.2.1. Microhardness testing

The hardnesses of finely-polished ribbon samples were measured both before and after heat treatments, in a Vickers microhardness tester (Vickers model M12a) using a load of 50 g, for 20 sec, on the as-received samples and the samples heated to 395 and 500° C. A load of 20 g, for 20 sec, was used on the samples annealed at 720 and 840° C. An average of twenty indentations were made for each sample analysed. For all the measurements the standard deviation of the values was less than 6% of the mean value.

Microhardness results are listed in Table II and are shown graphically in Fig. 8.

2.2.2. Saturation magnetization measurements

Saturation magnetization, $4\pi M_S$, measurements were made on both the as-received and heat-treated foils using a vibrating sample magnetometer. This magnetometer was calibrated using a cylinder of Ni, and the error in the measurement of the magnetic moment should be no greater than 1%. The volume of each sample was estimated by the ratio m/ρ, where m is the sample mass and ρ is the published density of amorphous $Fe_{80}B_{20}$ equal to 7.4 g cm^{-3}. During crystallization of amorphous alloys the density is expected to increase by, at most, 1% and therefore the $4\pi M_S$ error estimate was taken to be $\{^{+2\%}_{-1\%}\}$.

Variation in saturation magnetization values are plotted in Fig. 9 and are summarized in Table II. Table II also shows that the published value for the amorphous $Fe_{80}B_{20}$ sheets (1.56 T) agrees quite well with our measurements on the as-received material (1.546 T). The completely crystallized matrix, consisting of two-phase, α-Fe phase and Fe_2B phase, mixtures, exhibit a considerably higher (1.7316 T) saturation magnetization value, as shown.

3. Discussion

3.1. Structural analyses

A few compositional variables are seen to occur in both the production and the heat treatment of $Fe_{80}B_{20}$ alloy, depending on the rate of cooling

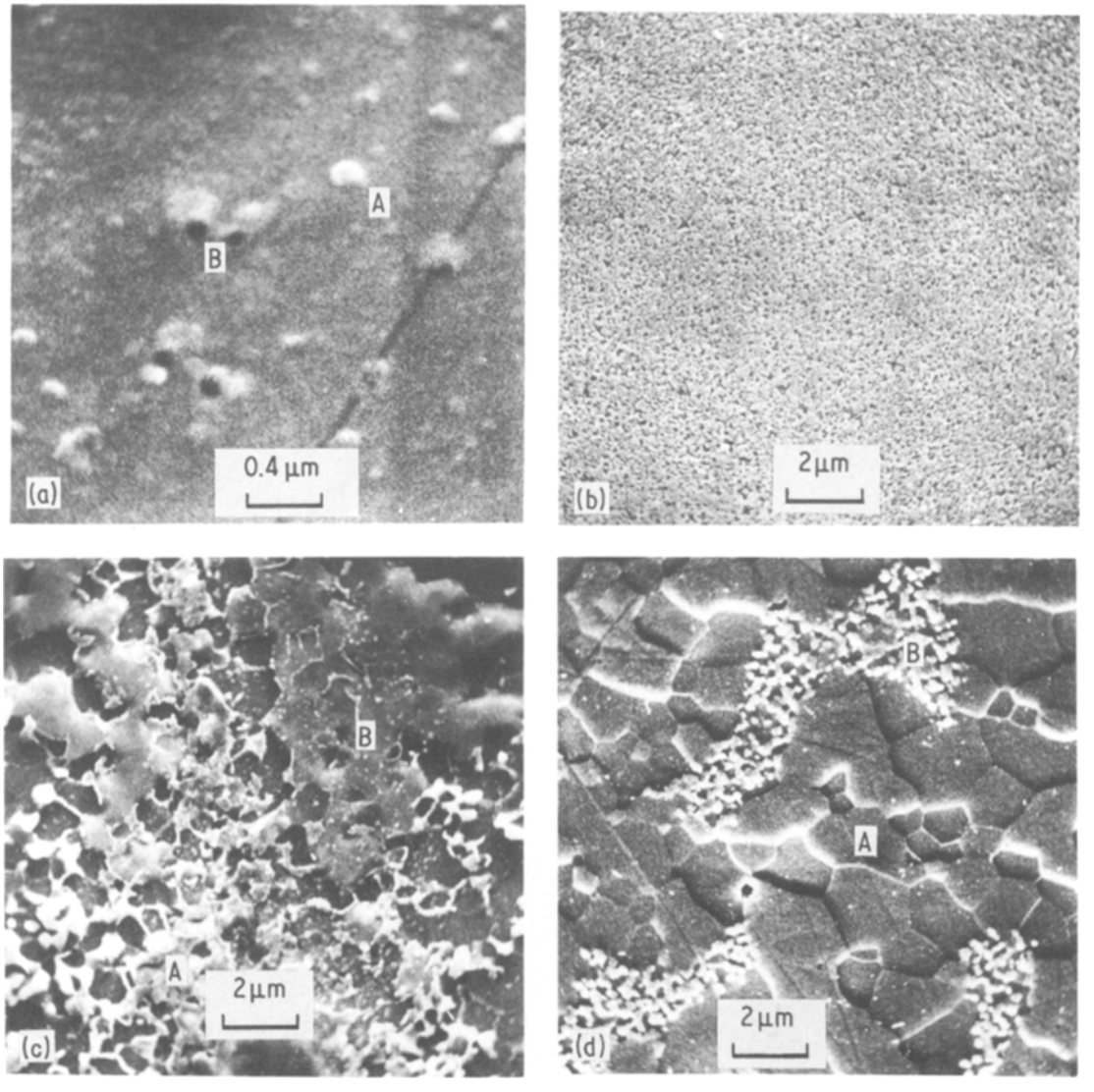

Figure 7 Scanning electron micrographs of $Fe_{80}B_{20}$ alloys annealed for 5 min in an inert atmosphere at (a) 395° C, (b) 500° C, (c) 720° C and (d) 840° C. (0.06 μm finish followed by etching in 1 vol% HNO_3 in methanol for 10 to 20 sec.)

and rate of heating to temperature, respectively. For example, only cooling rates from the melt greater than 10^{6}° C sec^{-1} are seen to produce the glassy structure while slow rates of cooling are seen to produce either a eutectic mixture of α-Fe and Fe_3B (orthorhombic) phases or platelets of Fe_3B phase imbedded in an amorphous matrix. Heat treatment, to induce crystallization, on the other hand, is seen to lead to the dissolution of the metastable matrix ($Fe_{\sim 3.5}B$) into Fe_3B phase plus α-Fe phase mixture, through a discontinuous reaction with a heating rate of 1° C sec^{-1} to 700° C while this structure is seen to dissolve into an equilibrium α-Fe phase plus Fe_2B phase mixture above 900° C. A much faster heating rate (reaching 900° C after 2 sec), in contrast, is seen to lead to the transformation of the metastable matrix $Fe_{\sim 3.5}B$ directly into the α-Fe plus Fe_2B equilibrium structure at 900° C [6–8]. In the study presented here, the initial wire and sheet samples were characterized to be fully amorphous, as indicated in Table I and the field ion micrograph shown in Fig. 2. The heating rates utilized in the annealing treatment were a constant 3 to 5° C min^{-1} throughout the study and the initial resistance survey was made at similar heating rates to avoid such discrepancies.

TABLE II Physical property alterations

Heat-treatment temperature (° C for 5 min)	Saturation magnetization (T)	Microhardness* (kg mm^{-2})
Amorphous (as-received)	1.546†	1044
395	1.6206	1264
500	1.6650	1260
720	1.7242	838
840	1.7316	679

*In all cases, the standard deviation of the measured values was less than 6% of the mean value.
†Value advertised by Allied Chemicals is 1.56 T for the amorphous, as-received, sheet.

3.1.1. Sample annealed at 395° C

X-ray diffraction data indicate a partial crystallization following heating at 395° C for five minutes with the resulting microstructure consisting of the product α-Fe and Fe_3B phases imbedded in the amorphous matrix. The diffraction patterns obtained clearly indicate the presence of crystallinity in this sample and when the background scattering levels of the patterns for samples annealed at 395 and 500° C are compared, the only difference observed is the extremely broadened lines of the sample annealed at 395° C. Line-broadening analysis [12] indicates that the particle size of the α-Fe crystals are about 10 nm and exhibit excessive deformation (strain) or faulting [13] (possibly twin faults). This is seen when the (1 1 0) reflection is compared with the (2 0 0) reflection in Fig. 10a, showing the diffraction pattern of the sample annealed at 395° C. (For comparison Fig. 10b shows the diffraction pattern of the amorphous sheet.) This plot shows the broad (1 1 0) peak and the relatively sharp (2 0 0) peak in the pattern of the sample annealed at 395° C that is quite unique and was not observed in our previous work [3, 14]. The fully crystallized sample obtained following annealing at 500° C, on the other hand, exhibits no line broadening.

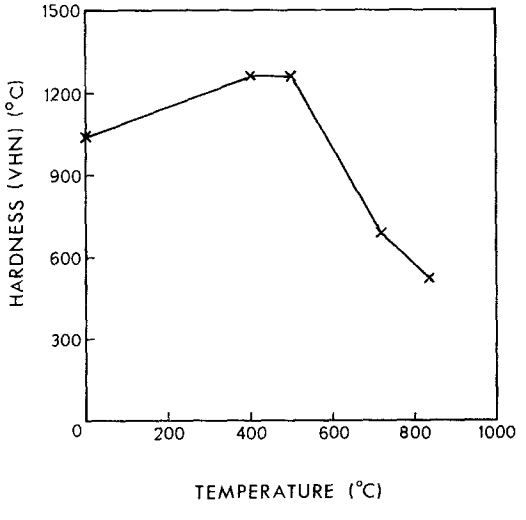

Figure 8 Variation in microhardness plotted against temperature of heat treatment (5 min at temperature).

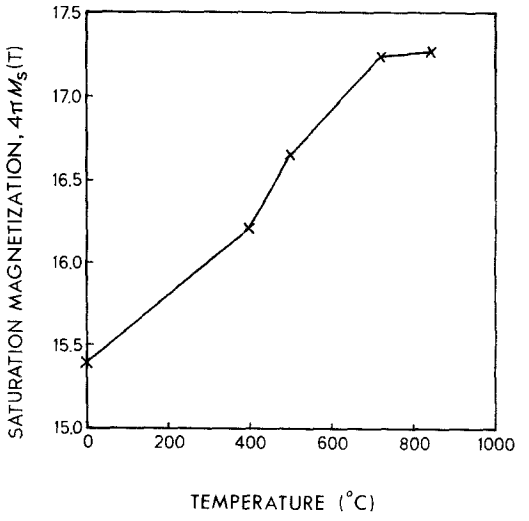

Figure 9 Variation of saturation magnetization ($4\pi M_S$) with heat treatment for $Fe_{80}B_{20}$ Metglas alloy. (Metglas is a registered trade name of the Allied Chemical Corp.)

In contrast to this observation, the first indication of twinning is observed in the field ion microscrope analyses following heat treatment at 720° C, as shown in Fig. 5. The crystallite dimension of the α-Fe, of about 10 nm, is consistent with the relative size given for these particles in earlier work [15]. This study [15] also mentions the lack of a sharp interface between the product phases and the amorphous matrix at this early stage of crystallization. This is seen to be the case with the structure shown in the scanning electron micrograph of the sample annealed at 395° C shown in Fig. 7a. This partial transformation is consistent with differential scanning calorimetry that indicates one-half transformation of $Fe_{80}B_{20}$ to the crystallized state after heat treatment for approximately 50 min at 390° C [4]. This three-phase mixture has also been observed after annealing $Fe_{80}B_{20}$ at 370° C [3] while a 2 h anneal at 370° C is reported to result in the complete crystallization of this alloy [8].

Imaging characteristics of the amorphous $Fe_{80}B_{20}$, as well as those of the product phases of transformation such as α-Fe, Fe_3B and Fe_2B, were elaborated upon in our original paper [3] and will

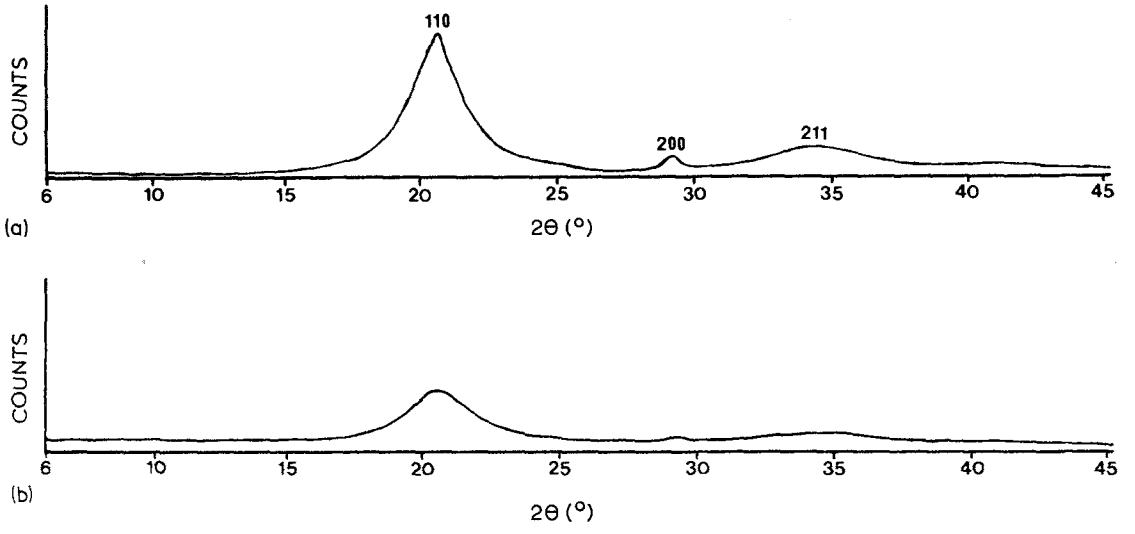

Figure 10 X-ray diffraction (diffractometer) patterns of $Fe_{80}B_{20}$ sheets: (a) sample annealed at 395° C for 5 min and (b) amorphous sample.

not be repeated here. There are, however, a few new features seen in the study now presented. One such feature is the eutectoid decomposition of the amorphous matrix into product phases of α-Fe and Fe_3B observed following heat-treatment at 395° C. Fig. 2 shows crystalline islands, consisting of iron clumps exhibiting the α-Fe phase and the more disperse atomic spots suggesting the low-symmetry Fe_3B phase, present in a dark back-ground matrix phase. This is indicative of the different best-image voltages that expose the product and the matrix phase structures. However, at the best-image voltage at which the back-ground could be imaged, the product phases were lost in these micrographs. This phenomenon was also observed in our earlier study following exposure for 5 sec of the amorphous material to 780° C, where the large clusters of α-Fe domains were lost in the atomic detail defining these surfaces because of the different imaging voltages.

3.1.2. Sample annealed at 500° C

X-ray diffraction analyses indicate that the amorphous alloy is fully crystallized following exposure for 5 min to 500° C with a resulting phase mixture of α-Fe and Fe_3B constituting the microstructure. To demonstrate that complete crystallinity has already taken place in a micro-structure, the following simple computation, based on X-ray diffraction data, was made. Since the overall chemical composition, expressed in atomic per cent of the alloy, is known and is expected to remain constant during the heat treatment, one can represent the total structure as being composed of volume fractions C_1 and C_2 for the α-Fe and Fe_3B phase, respectively, and in terms of numbers of atoms: $C_1(Fe_{100}) + C_2(Fe_{75}B_{25})$. Assuming a ratio $C_1/C_2 = 0.25$ gives:

$$0.2(Fe_{100}) + 0.8(Fe_{75}B_{25}) = Fe_{20} + Fe_{60}B_{20} = Fe_{80}B_{20},$$

which is the initial composition of the amorphous alloy. Using the direct comparison method [16], the existence of such a ratio was calculated from X-ray diffraction (diffractometer) data. For this calculation the unit-cell dimension and the crystal structure of the phases present in the microstructure must be known [17, 18]. Since C_1 and C_2 are the volume fractions (and in our case also the concentrations, the densities of α-Fe and Fe_3B phases being similar), the following relationships can be used to evaluate C_1 and C_2:

$$C_1/C_2 = \frac{I_1 R_2}{I_2 R_1} \quad (2)$$

and

$$C_1 + C_2 = 1, \quad (3)$$

where I is the integrated intensity of a diffraction profile $(h\,k\,l)$ and $R = v^{-2}|F|^2 p P_L$, where v is the unit-cell volume, F is the structure factor, p is the multiplicity factor and P_L is the Lorentz polarization factor. Our computation, with the experimental data, shows that the structure is fully crystallized after annealing at 500° C.

Although no direct heat treatment of the

amorphous $Fe_{80}B_{20}$ alloy at 500° C is referenced in the literature, it is indicated that heat treatment above 500° C results in coarsening of the α-Fe phase and a cessation of ordering in the metastable $Fe_{\sim 3.5}B$ phase [8].

The field ion micrograph in Fig. 4 shows the clusters of α-Fe phase in a matrix of Fe_3B phase comprising the microstructure. The partial ring structure observed throughout the micrograph suggests complete crystallinity of this structure. The relative ratio of the α-Fe clusters and the arrangement of the two phases in these micrographs is quite reminiscent of the structure obtained following exposure of the amorphous alloy to a temperature of 780° C for one second, and the heating rate in the latter case was instantaneous achievement of 780° C through resistive heating. This similarity could, of course, be coincidental but it is also indicative of the fact that the product phases are similar in these two transitions at different temperatures, rates of heating and isothermal treatments, thus suggesting the multi-faceted nature of the amorphous-to-crystalline transition in this alloy.

3.1.3. Sample annealed at 720° C

X-ray diffraction data indicates that the Fe_3B phase of the lower-temperature anneals is lost following the heat-treatment at 720° C and is replaced by a two-phase mixture of $Fe_{23}B_6$ and the Fe_2B phases while α-Fe seems to be unaltered. The appearance of the equilibrium phase Fe_2B following a heat treatment of 5 min at 720° C seems, initially, to be inconsistent with our first study where heat treatment for longer than 15 min was required at 780° C for the appearance of this phase through the reaction:

$$Fe_{80}B_{20}(\text{amorphous}) \rightarrow \alpha\text{-Fe} + Fe_3B\,(\text{p t}) \rightarrow Fe_2B\,(\text{b c t}). \quad (4)$$

The transformation at 720° C can thus be considered different in nature, since the reaction seen is:

$$Fe_{80}B_{20}(\text{amorphous}) \rightarrow \alpha\text{-Fe} + Fe_{23}B_6\,(\text{f c c}) \rightarrow Fe_2B\,(\text{b c t}). \quad (5)$$

This reaction proceeded during a much slower heating rate (3 to 5° C sec^{-1}) and yielded the phase $Fe_{23}B_6$ rather than Fe_3B. Much faster heating rates (1° C sec^{-1}) are seen to produce an α-Fe phase plus Fe_3B phase mixture [8] at 700° C. Fe_2B phase was also observed in previous work [10] following heat treatments of 2 h at temperatures between 600 and 700° C.

The metastable $Fe_{23}B_6$ phase has been observed following splat-cooling of $Fe_{95}B_5$ (together with α-Fe phase) [10] and following a 1 h anneal at 800° C (together with α-Fe and Fe_2B phases) and is considered isomorphous with f c c $Cr_{23}C_6$ structure [8, 10].

The field ion micrograph given in Fig. 6 shows a twin slice at an angle of 120° to the horizontal composed of α-Fe atoms of approximately 5 to 10 nm in width dividing the phase or phases to its right and left, possessing lower symmetry. If the $Fe_{23}B_6$ phase, indicated by the X-ray diffraction data, is present in this micrograph, the high symmetry (f c c) it should exhibit is not apparent either in this structure or in others that were analysed in this study. However, if the approximate amount of the $Fe_{23}B_6$ phase that could be expected is considered, its presence in this image, since it is a distinct phase separating Fe_2B and α-Fe domains [8], is unlikely or difficult to ascertain.

Twinning accompanying crystallization has been observed in $Fe_{80}B_{20}$ following a 2 h anneal at 380° C (on {2 1 1} planes of Fe_3B, dividing the crystal into quadrants) [19] but is obviously different in nature and consistency. The twin slices observed in our earlier study (following annealing at 780° C for 45 sec and 1 min) were also comprised of α-Fe atoms, made evident by their imaging characteristics [3].

3.1.4. Sample annealed at 840° C

X-ray diffraction analyses indicate the presence of the equilibrium phase mixture of α-Fe and Fe_2B phases in the microstructure following heat treatment for 5 min at 840° C. The structure obtained in the field ion microscope analyses (shown in Fig. 6) indicates some phase separation between the two phases, shown by the very bright clustering of α-Fe atoms separating domains of the Fe_2B phase. This is quite reminiscent of the structure obtained following the 1 h anneal at 780° C of our previous work. The same two crystalline product phases were seen in other work [8] following a fast heating (450° C sec^{-1}) to 900° C although other research shows that this mixture of phases is obtained only after an isothermal anneal of 2 h at 900° C [10]. We contend that the latter study reports a later stage of the transfor-

mation reaction (phase growth) rather than the formation of the initial crystalline products produced at this temperature. Another study reveals the product phases to be a eutectoid mixture of α-Fe and Fe_3B phases following an anneal of 1 h at 800° C [6] while the same phases are obtained in yet another study [7] following a heat treatment at 800° C for 5 min. It is generally concluded in this latter work [7] that heat treatment between 700 and 800° C produces a phase mixture of Fe_3B and α-Fe phases with the Fe_3B phase assuming an orthorhombic structure and that only anneals at temperatures above 1000° C produce the equilibrium structure of Fe_2B and α-Fe phases.

3.1.5. Discussion of structural analyses

Isothermal annealing at 780° C has indicated an amorphous-to-crystalline transition yielding an α-Fe plus Fe_3B phase mixture in the early stages of anneal (1 to 60 sec) followed by the gradual appearance and growth of the Fe_2B phase at the expense of the metastable Fe_3B phase, and the growth of the equilibrium α-Fe plus Fe_2B phase mixture (0.375 to 8 h) [3], indicating a transition of amorphous → Fe_3B → Fe_2B with no intermediary FeB compound formation. The present study shows a transformation of the amorphous alloy into an α-Fe phase and Fe_3B phase mixture at the lower temperatures of anneal (395 to 500° C) followed by a subsequent transformation of the metastable Fe_3B phase into a phase mixture of $Fe_{23}B_6$ and Fe_2B phases (at 720° C) which, in turn, transforms into the equilibrium phase mixture of α-Fe and Fe_2B (at 840° C). Hence, the reactions among the various metal–metalloid compounds proceeds as:

$$Fe_3B \rightarrow Fe_{23}B_6 \rightarrow Fe_2B. \qquad (6)$$

This reaction sequence is quite unique and different from that observed in our parallel study on $Fe_{40}Ni_{38}Mo_4B_{18}$ (Metglas* 2826 MB of Allied Chemical Corp.) [14]. In this study isothermal heating for 2 h at various temperatures (420, 500, 550, 670 and 800° C), isothermal transformation at 780° C for various durations and heating for 300 h at various temperatures (400, 600, 700 and 850° C) always indicated a transformation of the form:

$$Fe_xNi_{23-x}B_6 \rightarrow (Fe, Ni)_3B; \qquad (7)$$

i.e., the metastable face-centred cubic phase proceeds the appearance of the $metal_3$–metalloid compound. This could be explained as a feature of the one-metal–one-metalloid composition of the Fe–B alloy of the present study and is consistent with previous work [8].

3.2. Physical property evaluations

3.2.1. Microhardness

The initial increase in the microhardness value following heating at 395° C is another indication of the initiation of crystallization in the amorphous alloy, and is consistent with previous work [10]. The maintenance of the same value at 500° C, where crystallization was observed to be complete, suggests that the microhardness measurement is not sensitive enough to delineate the structural differences observed between the two product microstructures indicated earlier.

The decrease in hardness following heating at 720° C supports earlier work that suggests that the Fe_2B and $Fe_{23}B_6$ phases are not as hard as the Fe_3B phase [8]. The further hardness decrease following the 720° C anneal can be attributed to the coarsening of the α-Fe and Fe_2B phases rather than to the disappearance of the $Fe_{23}B_6$ phase; it is quite obvious that the amount of the $Fe_{23}B_6$, seen following annealing at 720° C, is not sufficient to cause such a drop in the microhardness value with its disappearance. Coarsening-induced hardness reductions have also been observed in previous work on this alloy [8] and other crystallized metallic glass structures [14].

3.2.2. Saturation magnetization

The absence of long-range atomic order and the consequent lack of magneto-crystalline anisotropy in ferrous metallic glasses result in materials having low coercive forces and core losses. In particular, $Fe_{80}B_{20}$ has been shown to have a core loss substantially lower than typical iron-based crystalline alloys at comparable flux levels, including saturation [20].

The saturation magnetization of $Fe_{80}B_{20}$ was expected to change upon crystallization into the equilibrium structure of α-Fe and Fe_2B. Since the saturation magnetization of both of these phases is available in the literature, it is possible to estimate the saturation magnetization for crystallized $Fe_{80}B_{20}$. The magnetic moment of Fe_2B [16] is 1.91 Bohr magnetons Fe-atoms^{-1} [21].

*Metglas is a registered trade name of the Allied Chemical Corp.

Using crystallographic data from Taylor and Kagle [22] and the conversion factor: 1 Bohr magneton = 9.274×10^{-24} J T^{-1}, we calculate the saturation magnetization of Fe_2B to be 1.6046 T. The saturation magnetization of α-Fe is reported to be 2.1580 T [23]. If the volume fraction of the equilibrium phases were known, an estimate of the saturation magnetization of crystallized $Fe_{80}B_{20}$ could be made using the rule of mixtures. Again using crystallographic data [22] and assuming

$$80\,\text{vol}\%\ \text{Fe}\ 20\,\text{vol}\%\ \text{B} \rightarrow 20\,\text{vol}\%\ \text{Fe}_2\text{B} + 40\,\text{vol}\%\ \text{Fe}, \quad (8)$$

the volume fraction of α-Fe is calculated to be 0.459. This simple estimate yields a saturation magnetization for crystallized $Fe_{80}B_{20}$ of 1.8586 T which is in reasonable agreement with the measured value of 1.7316 T. This increased saturation magnetization with increasing crystallization is consistent with the behaviour of the 2826 MB alloy observed in our parallel study [14].

4. Conclusions

The main conclusions that are derived from the study are:

(a) The temperatures where phase transitions have been observed in the continuous heating of amorphous $Fe_{80}B_{20}$ are 395, 500, 720 and 840° C.

(b) The transformations observed were in the sequence of: amorphous $\rightarrow Fe_3B \rightarrow Fe_{23}B_6 + Fe_2B \rightarrow Fe_2B$, with the primary α-Fe phase being present in each step of the crystallization procedure.

(c) Micro-hardness has been seen to increase upon initiation of crystallization but is seen to drop following completion of crystallization with the achievement of the equilibrium phase mixture and the ensuing coarsening of each phase.

(d) Saturation magnetization values have been seen to increase (by approximately 12%) with increasing degree of crystallization; the highest rate of increase of saturation magnetization was observed in the initial stages of crystallization.

Acknowledgements

Partial support for this research was received from the Research and Development Division of NMIMT and this support is gratefully acknowledged.

References

1. R. E. MARINGER and C. E. MOBLEY, *J. Vac. Sci. Technol.* **11** (1974) 1067.
2. P. CHAUDHARY, B. C. GIESSEN and D. TURNBULL, *Sci. Amer.* **242** (1980) 98.
3. O. T. INAL, L. KELLER and F. G. YOST, *J. Mater. Sci.* **15** (1980) 1947.
4. L. A. DAVIS, R. RAY, C. P. CHOU and R. C. O'HANDLEY, *Scripta Met.* **10** (1976) 541.
5. M. M. KARNOWSKY, *J. Mater. Sci.* **13** (1978) 2339.
6. U. HEROLD and U. KOSTER, Proceedings of the 3rd International Conference on Rapidly Quenched Metals, Brighton, July, 1978, Vol. II, p. 281.
7. U. KOSTER and U. HEROLD, *Scripta Met.* **12** (1978) 75.
8. U. HEROLD and U. KOSTER, *Z. Metallkde.* **69** (1978) 326.
9. J. L. WALTER, S. F. BARTRAM and R. R. RUSSELL, *Met. Trans. A* **9A** (1978) 803.
10. H. FRANKE, U. HEROLD, U. KOSTER and M. ROSENBERG, Proceedings of the 3rd International Conference on Rapidly Quenched Metals, Brighton, July, 1978, Vol. I, p. 155.
11. O. T. INAL and L. E. MURR, *J. Appl. Phys.* **49** (1978) 2427.
12. A. R. STOKES, *Proc. Phys. Soc. Lond.* **61** (1948) 382.
13. B. E. WARREN, "X-ray Diffraction" (Addison-Wesley Pub. Co., New York, 1969).
14. K. P. MIZGALSKI, O. T. INAL, F. G. YOST and M. M. KARNOWSKY, unpublished work, 1981.
15. H. FUJITA and K. HASHIMOTO, *Mater. Sci. Eng.* **45** (1980) 221.
16. B. D. CULLITY, "Elements of X-ray Diffraction", 2nd Edn (Addison Wesley Pub. Co., New York, 1978).
17. R. G. WYCKOFF, "Crystal Structures", 2nd Edn (Wiley-Interscience, New York, 1964).
18. F. M. NORMAN, H. LONGSDALE and K. LONGSDALE, "International Tables for X-ray Crystallography" Vol. 1 (Kynock Press, Birmingham, 1952).
19. F. E. LUBORSKY, *Mater. Sci. Eng.* **28** (1977) 129.
20. F. E. LUBORSKY, P. G. FRISCHMANN and L. A. JOHNSON, *J. Magnetism and Magnetic Mater.* **8** (1978) 318.
21. R. M. BOZORTH, "Ferromagnetism" (Van Nostrand Inc., New York, 1951) p. 224.
22. A. TAYLOR and B. J. KAGLE, "Crystallographic Data on Metal and Alloy Structures" (Dover Publications Inc., New York, 1963) p. 195.
23. R. M. BOZORTH, "Ferromagnetism" (Van Nostrand Inc., New York, 1951) p. 867.

Received 5 March and accepted 29 April 1981.